Inorganic Chemistry

Article

pubs.acs.org/IC

Synchrotron-based Nickel Mössbauer Spectroscopy

Leland B. Gee,[¶] Chun-Yi Lin,[¶] Francis E. Jenney, Jr.,[§] Michael W.W. Adams,[§] Yoshitaka Yoda,[¥] Ryo Masuda,[‡] Makina Saito,[‡] Yasuhiro Kobayashi,[‡] Kenji Tamasaku,[◇] Michael Lerche,[¶] Makoto Seto,[‡,†] Charles G. Riordan,[∞] Ann Ploskonka,[∞] Philip P. Power,[¶] Stephen P. Cramer,*[,¶,£] and Lars Lauterbach[€,¶]

[¶]Department of Chemistry, University of California, Davis, California 95616, United States

[§]Georgia Campus, Philadelphia College of Osteopathic Medicine, Suwanee, Georgia 30024, United States

[¥]Japan Synchrotron Radiation Research Institute (JASRI), SPring-8, 1-1-1 Kouto, Sayo-gun, Hyogo 679-5198, Japan

[‡]Research Reactor Institute, Kyoto University, Kumatori-cho, Sennan-gun, Osaka 590-0494, Japan

[◇]SR Material Science Inst. Unit, RIKEN SPring-8 Center, 1-1-1 Kouto, Sayo, Hyogo 679-5148, Japan

[†]Japan Atomic Energy Agency, Mikazuki-cho, Sayo-gun, Hyogo 679-5148, Japan

[∞]Department of Chemistry & Biochemistry, University of Delaware, Newark, Delaware 19716, United States

[£]Physical Biosciences Division, Lawrence Berkeley National Laboratory, Berkeley, California 94720, United States

[€]Department of Chemistry, Technische Universtät Berlin, Strasse des 17. Juni 135, 10623 Berlin, Germany

Supporting Information

ABSTRACT: We used a novel experimental setup to conduct the first synchrotron-based ^{61}Ni Mössbauer spectroscopy measurements in the energy domain on Ni coordination complexes and metalloproteins. A representative set of samples was chosen to demonstrate the potential of this approach. $^{61}NiCr_2O_4$ was examined as a case with strong Zeeman splittings. Simulations of the spectra yielded an internal magnetic field of 44.6 T, consistent with previous work by the traditional ^{61}Ni Mössbauer approach with a radioactive source. A linear Ni amido complex, $^{61}Ni\{N(SiMe_3)Dipp\}_2$, where Dipp = C_6H_3-2,6-$^iPr_2$, was chosen as a sample with an "extreme" geometry and large quadrupole splitting. Finally, to demonstrate the feasibility of metalloprotein studies using synchrotron-based ^{61}Ni Mössbauer spectroscopy, we examined the spectra of ^{61}Ni-substituted rubredoxin in reduced and oxidized forms, along with $[Et_4N]_2[^{61}Ni(SPh)_4]$ as a model compound. For each of the above samples, a reasonable spectrum could be obtained in ∼1 d. Given that there is still room for considerable improvement in experimental sensitivity, synchrotron-based ^{61}Ni Mössbauer spectroscopy appears to be a promising alternative to measurements with radioactive sources.

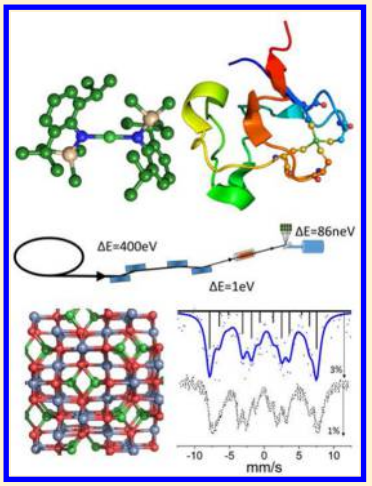

INTRODUCTION

Despite the importance of Ni chemistry to materials[1] and battery science,[2] catalysis,[3] inorganic chemistry,[4] and bioinorganic chemistry,[5−7] there are relatively few reports on ^{61}Ni Mössbauer spectroscopy. Specifically, there are tens of thousands of papers reporting the application of ^{57}Fe Mössbauer spectroscopy, while the ^{61}Ni Mössbauer literature can be counted in the dozens. The reason for this discrepancy is clear—compared to ^{57}Fe experiments, traditional Mössbauer spectroscopy using the ^{61}Ni 67.4 keV nuclear resonance is logistically difficult.[8] The most appropriate parent isotopes, ^{61}Co or ^{61}Cu, have lifetimes of 99 m or 3.3 h, respectively, requiring that experiments be done with frequent source changes and in close proximity to proton cyclotrons or electron accelerators, where the sources are produced.[8−11]

Time-domain approaches using synchrotron radiation[12] can in principle yield the same information as energy domain Mössbauer experiments. For example, nuclear forward scattering (NFS) has been used to study Ni metal at low temperatures[13] and under high pressure,[14] and synchrotron radiation perturbed angular correlation (SRPAC) measurements on Ni metal have also been successful.[15] However, the interpretation of such time-domain measurements is not always straightforward, especially for mixtures. The popularity of ^{61}Ni nuclear spectroscopy would certainly benefit from a better energy domain experiment that can be interpreted by standard Mössbauer procedures. Improvements in synchrotron X-ray generation and detection have recently made just such an experiment possible.

Energy-domain synchrotron radiation Mössbauer spectroscopy (SR-MS), first proposed in 1974,[16] was first conducted in 1985[17] using an ^{57}Fe-yttrium iron garnet nuclear Bragg diffraction monochromator.[17] Monochromator development

Received: December 31, 2015
Published: July 7, 2016

DOI: 10.1021/acs.inorgchem.5b03004
Inorg. Chem. 2016, 55, 6866−6872

Scheme 1. Synchrotron Radiation Mössbauer Spectroscopy Experiment

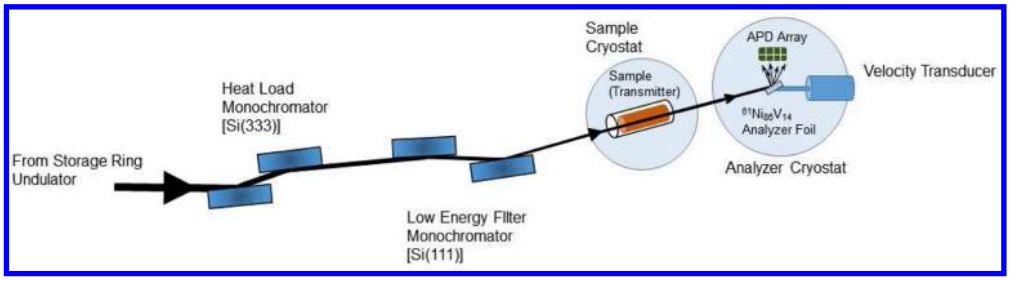

Table 1. Comparison of Mössbauer-Relevant Nuclear Properties for ^{57}Fe and ^{61}Ni

	abundance (%)	E (keV)	$t_{1/2}$ (ns)	2Γ (mm s^{-1})	I_g	I_e	α_t	μ_g (n.m.)	μ_e (n.m.)	Q_g (barn)	Q_e (barn)
^{57}Fe	2.14	14.41	97.81	0.194	1/2$^-$	3/2$^-$	8.21	0.0906	−0.155		0.16
^{61}Ni	1.19	67.40	5.27	0.77	3/2$^-$	5/2$^-$	0.12	−0.749	0.481	0.162	−0.2

continued with work using a single-line $^{57}FeBO_3$ monochromator.[18,19] However, this diffraction approach requires near-perfect isotopically enriched single crystals with favorable magnetic properties,[17,20−22] and until now it has only been achieved with ^{57}Fe. An alternate approach to SR-MS uses a moderately monochromatic synchrotron beam as the source and a single-line Mössbauer isotope as analyzer (Scheme 1). It was first demonstrated in 2009 by Seto and co-workers on ^{57}Fe and ^{73}Ge.[23] It has since been applied to ^{151}Eu,[24] ^{174}Yb,[25] ^{125}Te,[25] and ^{40}K,[26] and it has been proposed for nearly two dozen lanthanide isotopes.[25] Recently, Seto and co-workers have applied ^{61}Ni SR-MS to cathode materials[27] and nanoparticles.[28] This SR-MS approach is well-suited to nuclei with lifetimes shorter than the typical ∼10−100 ns electron bunch spacing in a synchrotron, that is, the time between radiation pulses.

The ^{61}Ni nucleus, with an excited-state $t_{1/2}$ = 5.27 ns, is an excellent candidate for SR-MS. Since ^{61}Ni Mössbauer is relatively unfamiliar to chemists, we first compare the spectroscopic properties of this isotope with the more familiar ^{57}Fe. The key nuclear properties are summarized in Table 1, and we briefly discuss some of the spectroscopic consequences below.

Lifetime and Energy. The most obvious differences between ^{61}Ni and ^{57}Fe are the energy and lifetimes of the first excited states. The long lifetime (98 ns) and low energy (14.4 keV) of the ^{57}Fe excited state lead to a natural line width 2Γ of 9.1 neV, while the shorter lifetime (5.3 ns) and higher energy of the ^{61}Ni resonance (67.4 keV) lead to spectral features with a line width of 173 neV, nearly a factor of 20 broader.

Isomer Shift (δ_{IS}). For ^{61}Ni, there is a smaller change in nuclear mean square radius ($\Delta\langle r^2\rangle/\langle r^2\rangle$) and higher transition energy, and these lead to a significant reduction in the ^{61}Ni isomer shift range, especially when expressed in terms of millimeters per second Doppler shift. Whereas common ^{57}Fe δ_{IS} values vary from −0.8 to +2.0 mm/s,[9] the range for ^{61}Ni δ_{IS} is ∼30-fold smaller, from −0.06 to +0.04 mm/s.[29] This is more than an order of magnitude smaller than the natural line width 2Γ = 0.77 mm/s. Moreover, the high energy for this transition (67.4 keV) requires corrections for second-order Doppler shifts that are of comparable magnitude to the real chemical isomer shifts.[29] Although such corrections are possible if the lattice dynamics are well-understood, as described by Gütlich,[29] that author has noted that so far, "the information concerning chemical bond properties was not very impressive."[29] For these reasons, in this work we have not tried to exploit ^{61}Ni isomer shifts (although others might do so in the future).

Magnetic Properties. The ^{61}Ni nucleus has favorable magnetic properties. It has relatively large magnetic moments in its ground and excited states, μ_g = −0.75 and μ_e = 0.48 nuclear magnetons (n.m.),[29] compared to μ_g = +0.09 and μ_e = −0.15 n.m. for ^{57}Fe (Table 1). Previous work with mixed spinel type oxides, such as $Cu_{0.9}Ni_{0.1}Cr_2O_4$, exhibited very large splitting of ±13.6 mm/s.[30] Since many of the interesting problems in Ni chemistry can be framed as questions about magnetic properties, this makes observation of Zeeman splittings in ^{61}Ni Mössbauer spectra one of the most promising applications.

Quadrupole Splittings. For ^{57}Fe, the transition is from I = 1/2 → I = 3/2. Since only the excited state is split by an electric-field gradient (EFG), ^{57}Fe Mössbauer often presents a symmetric doublet spectrum. The ^{61}Ni resonance involves an I = 3/2 → I = 5/2 transition. The quadrupole splitting is more complex, as the ground state (I = 3/2) and excited state (I = 5/2) yield two and three states, respectively (Figure S1), for five nonforbidden transitions. Although the five transitions for ^{61}Ni are not usually resolved, they can in principle provide more robust information than ^{57}Fe through the asymmetry of the quadrupole split spectrum (for axial systems), which is characterized by the sign of the V_{zz} component of the EFG and the asymmetry parameter η.

In this study we recorded SR-MS on a ferromagnetic nickel spinel—$^{61}NiCr_2O_4$, two coordination complexes with, respectively, linear and tetrahedral geometries—^{61}Ni[N(SiMe$_3$)C$_6$H$_3$-2,6-Pr$_2$]$_2$ and [Et$_4$N]$_2$[^{61}Ni(SPh)$_4$], and a Ni protein—Ni-substituted rubredoxin. The data for these samples showcases the sensitivity of ^{61}Ni SR-MS to the Ni internal magnetic hyperfine field, as well as to both the magnitude and the sign of the EFG. The results also demonstrate that the SR-MS can be used on dilute samples such as Ni proteins—the technique should eventually be useful for catalytic studies of hydrogenase, which contain a NiFe heteronuclear bimetallic cofactor in their active site.

EXPERIMENTAL METHODS

Synthesis of $NiCr_2O_4$. $^{61}NiCr_2O_4$ (**1**) was produced from 99% enriched ^{61}Ni (Isoflex) and Cr_2O_3 powders. Following a previously established procedure, the two powders were mixed in an agate mortar and sintered twice in a conventional vertical furnace at atmospheric pressure and 1200 °C for 24 h in air.[31] The sample composition was confirmed by powder X-ray diffraction.

DOI: 10.1021/acs.inorgchem.5b03004
Inorg. Chem. 2016, 55, 6866−6872

Synthesis of $^{61}NiBr_2(OEt_2)$. In a Schlenk flask, ^{61}Ni metal (0.051 g, 0.84 mmol) in ca. 10 mL of Et_2O and excess Br_2 (1.36 g, 8.51 mmol) were added via a syringe.[32] The reaction mixture was stirred for 16 h without light. The insoluble $^{61}NiBr_2(OEt_2)$ was allowed to settle and filtered through a filter cannula. The residue was washed twice with Et_2O and dried under vacuum to afford 0.206 g (0.699 mmol) of $^{61}NiBr_2(OEt_2)$.

Synthesis of $^{61}Ni\{N(SiMe_3)Dipp\}_2$. $^{61}Ni\{N(SiMe_3)Dipp\}_2$ (**2**) (where Dipp = C_6H_3-2,6-$^iPr_2$), 0.375 g (1.47 mmol) of $LiN(SiMe_3)$-Dipp, and 0.206 g (0.699 mmol) of $^{61}NiBr_2(OEt_2)$ were combined as solids in a Schlenk flask, and 30 mL of Et_2O was added at ca. 0 °C.[33] The reaction mixture quickly turned purple and was allowed to warm to room temperature and stirred for 18 h. All volatile material was removed under vacuum, and the residue was extracted with ca. 30 mL of pentane. The solution was filtered through a filter cannula, and the filtrate was concentrated to incipient crystallization. Storage at −80 °C for 1 d afforded 0.172 g (0.308 mmol) of crystals.

Synthesis of $[Et_4N]_2[^{61}Ni(SPh)_4]$. $[Et_4N]_2[^{61}Ni(SPh)_4]$ (**3**) was prepared as described previously,[34] with the following modifications: ^{61}Ni-labeled $[Et_4N]_2(NiCl_4)$ was used as a reagent; $[Et_4N]_2[NiCl_4]$ and $[Et_4N]SPh$ were combined in acetonitrile rather than propionitrile and stirred for 4 h at room temperature, isolated by filtration, and then washed with cold acetonitrile.

^{61}Ni-Substituted Rubredoxin Purification and Preparation. *Pyrococcus furiosus* rubredoxin (*Pf* Rd) was isolated and purified according to Jenney and Adams.[35] The Ni form of *Pf* Rd (Ni Rd) was prepared essentially according to Moura et al.[36] except that ^{61}Ni powder was dissolved in aqua regia and then neutralized with NaOH before addition to the denatured protein. Oxidized protein was prepared by treatment with 5 mM $K_3[Fe(CN)_6]$, which was removed by buffer exchange. The samples were prepared by exchange into Tris buffer (100 mM, pH 8.5) and by repeated concentration/dilution using a Centricon YM3 concentrator (Amicon). The final sample concentrations were 5−6 mM. Reduced samples contained 10 mM dithionite.

Synchrotron-based ^{61}Ni Mössbauer Spectroscopy. Samples were prepared in 2.0 mm inner diameter (ID) quartz tubes (for compounds **1**, **2**, and **3**) or 1.45 mm ID (for rubredoxins). The outer diameter was 3 mm. The path lengths were 2 mm for **1**, 2 cm for **2** and **3**, and 10 cm for the rubredoxin samples. The longer path length for the rubredoxin samples helped compensate for the lower ^{61}Ni concentrations. We note that the small divergence of a synchrotron beam allows the use of long narrow capillaries that would not be practical with radioactive sources (because extreme collimation would reduce the flux throughput from a radioactive source.)

The quartz sample cells were placed inside a 1 cm × 1 cm × 20.2 cm Cu block, which contained a cavity with a diameter of 3.3 mm. A temperature probe was attached to the surface of the coldfinger. The entire setup was shielded by a second Cu case with Al foil windows, which allowed for temperatures as low as 5 K.

All of the spectra were recorded using the approach illustrated in Scheme 1. The SPring-8 storage ring was running in the A bunch mode with 203 bunches spaced at 23.6 ns and a total current of 100 mA. Measurements (except for compound **3**) were taken at BL19LXU, where the synchrotron radiation comes from a 27 m undulator,[37,38] and the experimental setup was similar to that previously described.[23] The spectrum for **3** was collected at BL09XU with a 4.5 m long standard undulator and an otherwise identical setup.[39,40] The ninth undulator harmonic was first monochromated by a Si(333) high heat load monochromator, followed by a Si(111) low-energy filtering monochromator yielding a bandwidth of 2.3 eV with a flux of 2.2 × 10^{11} photons per second (4.3 eV with a flux of 1.0 × 10^{11} photons per second for BL09XU) at 67.4 keV. The radiation impinged on the sample in the coldfinger, and the transmitted photons then passed to a second cryostat containing a $^{61}Ni_{0.86}V_{0.14}$ analyzer foil mounted onto a velocity transducer. The radiative decay of the analyzer including photons and electrons, through nuclear fluorescence and internal conversion, was captured by an eight-element Si avalanche photodiode (APD) array. The APDs were gated to restrict the collection time to between 3 and 18 ns after the prompt pulse to discriminate against electronic scattering unrelated to the Mössbauer effect. The resulting spectrum is a function of the analyzer Doppler velocity, and is nearly identical to a conventional Mössbauer spectrum.

The spectra were simulated using a mixed magnetic and quadrupole Hamiltonian as implemented in the MossWinn software.[41−43] Fitting parameters can be found in Tables S1−S5.

RESULTS

$^{61}NiCr_2O_4$. Our synchrotron Mössbauer spectrum for **1** is shown in Figure 1. It exhibits a well-resolved Zeeman splitting

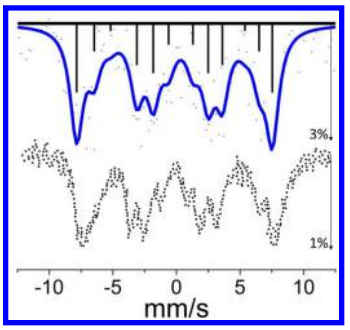

Figure 1. (top) The experimental SR-MS spectrum of $NiCr_2O_4$ powder (points) and a simulation (solid line) using an internal hyperfine field of 44.6 T. The pattern of four sets of three partially resolved magnetic hyperfine lines results from Zeeman splitting of I = 3/2 ground state and I = 5/2 excited state. The sticks represent individual transition contributions, solid line represents the fit, and dots indicate actual data. The maximum intensity decrease was ∼3% (indicated by downward arrow). (bottom) A recreation of the previously reported spectrum obtained with a radioactive source.[46]

indicating a significant internal magnetic field in this ferromagnetic sample, which is a spinel with high-spin Ni(II) in the tetrahedral sites. There are 12 magnetically split transitions for ^{61}Ni, and the spectrum can be described as four sets of three partially resolved lines. The fit was fixed to an axial EFG as in previous studies.[44,45] The fit yielded an internal hyperfine magnetic field of 44.6 T, in agreement with the value (44.5 T) from previous Mössbauer studies using radioactive ^{61}Co in a $^{62}Ni_{0.85}Cr_{0.15}$ source that was activated by bremsstrahlung.[46] V_{zz} was fit to 7.23 V/m^2; however, the fit was largely invariant of the V_{zz} value due to the quality of the data and the small effect of the EFG relative to the large internal magnetic field.

$^{61}Ni\{N(SiMe_3)Dipp\}_2$. The spectrum for **2** at 4.2K is broad and asymmetric (Figure 2). The spectrum was fit with an axial EFG (Table S2), and from this simulation we found that the asymmetry can be explained by a strong quadrupole splitting with a V_{zz} EFG component of 11.53 × 10^{21} V/m^2 at 4.2 K (The eQV_{zz} value for the ground state in mm/s is provided in Table S2). We also examined the temperature dependence of the spectral intensity, by taking additional data at 15, 30, and 40 K (Figure 2 and Figure S4). The rapid decline in intensity with increasing temperature illustrates the importance of the Lamb−Mössbauer factor for this high-energy transition and underlines the importance of conducting experiments at near LHe temperatures. Since linear Ni(II) complexes show pronounced changes in magnetic properties between 4 and 40 K,[47] the possible relevance of variable Zeeman splittings should be considered for detailed interpretation of the temperature-dependent spectra. We decided that better signal-to-noise is required for such an analysis.

DOI: 10.1021/acs.inorgchem.5b03004
Inorg. Chem. 2016, 55, 6866−6872

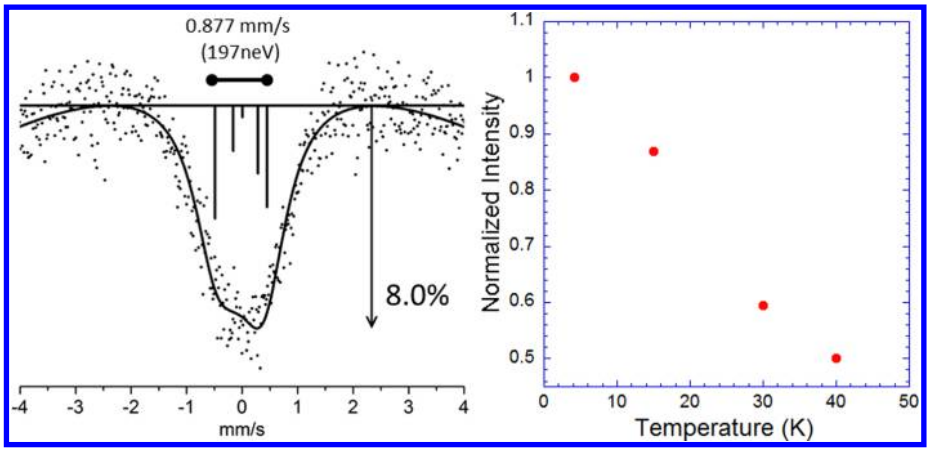

Figure 2. (left) The ^{61}Ni Mössbauer spectrum for the linear nickel complex **2**. The solid line represents the fit, and the vertical lines represent the energy and relative intensity of the individual transitions. The distance between the furthest transitions is shown above the spectrum (in mm/s and neV). (right) A plot of the normalized integrated intensity for 4.2, 15, 30, and 40 K relative to the 4.2 K integrated intensity.

^{61}Ni-Substituted *Pf* Rubredoxin and 3. The ^{61}Ni Mössbauer spectra for reduced and oxidized Ni Rd are compared with **3** in Figure 3, and fit parameters can be found in Table S3. The high quality of the spectra allowed them to be fit with a curved baseline to capture some of the well-known time window effect inherent in delayed coincidence Mössbauer and SR-MS.[48,49] The simulation for reduced Ni Rd resulted in a negative value for the V_{zz} component of the EFG, -11.2×10^{21} V/m^2 (η = 0.24). In contrast, the oxidized rubredoxin data were best simulated with a positive V_{zz} component; however, a large asymmetry parameter, (7.6×10^{21} V/m^2 η = 0.83), consistent with higher spherical symmetry of the EFG than the reduced sample. The spectrum for **3** was best simulated by a V_{zz} component of 10.8×10^{21} V/m^2 (η = 0.000). Our results cannot exclude modest magnetic effects from a slow paramagnetic relaxation and alternative fits are supplied in Table S4.

DISCUSSION

In this work, we reported the first energy domain synchrotron Mössbauer spectra for ^{61}Ni coordination complexes and metalloproteins, with samples chosen for extremes of Zeeman splitting, quadrupole splitting, or dilution. Our first sample was nickel chromite, $NiCr_2O_4$, **1**. This is a normal spinel with high-spin Ni^{2+} in the tetrahedral A sites and Cr^{3+} in the octahedral B sites. Apart from applications as an NOx sensor, a high emissivity coating, and as a catalyst, it has a rich variety of structural and magnetic phase transitions.[31] For our current purposes, it served as a test for the ability of SR-MS to span a wide range of resonances caused by a large Zeeman splitting.

As was documented in Figure 1, our instrument was capable of recording Zeeman splittings out to ±10 mm/s, which arise from the internal magnetic field of ~44.6 T. The signal-to-noise could certainly have been improved with more beam time. However, an unexpected benefit of the wide range of the data was that the magnetic field derived from a least-squares refinement was tightly constrained by the intensity in the wings of the spectrum and in good agreement with the previous result of 44.5 T.[46] In the future, SR-MS will be a useful probe of magnetic properties.

Our second sample was ^{61}Ni{N(SiMe$_3$)Dipp}$_2$, **2**, a high-spin linear Ni(II) complex. It belongs to a class of two-coordinate open-shell transition metal complexes with interesting magnetic

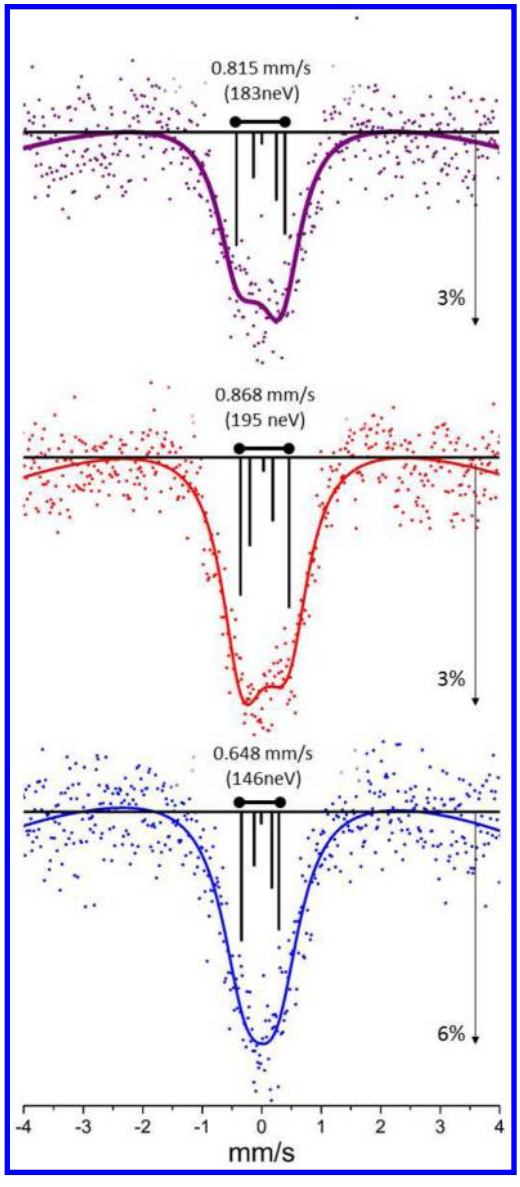

Figure 3. (top to bottom) ^{61}Ni SR-MS spectra for **3**, reduced, and oxidized ^{61}Ni *Pf* Rd. The sticks represent individual transition contributions to the simulation using parameters from Table S3.

DOI: 10.1021/acs.inorgchem.5b03004
Inorg. Chem. 2016, 55, 6866−6872

and catalytic properties (see ref 50 for references). For our current purposes this served as a system likely to have a strong quadrupole splitting. Although we could not resolve discrete transitions, we observed a strong asymmetry in the ^{61}Ni Mössbauer spectrum for **2**, especially at ∼4.2 K (Figure 2). The magnitude and sign of V_{zz} derived from the simulation (+11.5 × 10^{21} V/m^2) is consistent with our predicted value. For **2**, using the d-electron orbital energy order described previously,[33] the expectation value prediction of V_{zz} = +(4/7)e $\langle r^{-3}\rangle_{3d}$. However, it is important to note, for the interpretation of real data the sign of V_{zz} loses meaning as η approaches unity. Our attempts to record and interpret the temperature dependence of the spectra for **2** were less convincing. The signal dropped more than threefold between 4 and 40 K, illustrating the dramatic temperature dependence of the Lamb−Mössbauer factor at 67.4 keV.

Our final set of samples consisted of Ni(II) and Ni(III) *Pf* rubredoxin (Ni *Pf* Rd) and the model compound **3**. In the small (6 kDa) *Pf* Rd protein, the natural Fe center was replaced with Ni, yielding a high-spin Ni(II) center with four cysteine thiolate ligands in an elongated tetrahedral conformation.[51] The Ni site bears some resemblance to the active site Ni in NiFe H_2ases, where the Ni also has four cysteine ligands, two of them bridged to Fe.[52] Ni(II) *Pf* Rd can be oxidized to Ni(III) with ferricyanide,[53] and based on similar EPR signals, oxidized Ni Rd has been proposed as a model for the electron paramagnetic resonance (EPR) active Ni−C form of [NiFe] hydrogenases.[51] It was recently shown that Ni *Pf* Rd shows high hydrogen turnover frequencies (20−100 s^{-1}), admittedly with a large overpotential of 540 mV.[54] Our final sample, **3**, has been proposed as a model for Ni(II) Rd, as it also has a high-spin Ni(II) with distorted tetrahedral thiolate ligation.[55] For **3**, the distortion is an axial compression as opposed to the elongation in Ni(II) *Pf* Rd. For our current purposes, although interesting in their own right, these three samples are also obvious stepping stones to ^{61}Ni Mössbauer of NiFe H_2ases and other Ni enzymes.

As mentioned in the Introduction, ^{61}Ni has quadrupole moments of 0.16 and −0.20 barns, respectively, for the I = 3/2 ground and I = 5/2 nuclear excited states. This leads to five allowed transitions in a purely quadrupole split spectrum (Supporting Information, Figures S1 and S2). Using a single electron approximation for d-electrons and a simple crystal field model, as discussed previously,[29] we can predict the sign of the expectation value for V_{zz} based on geometry. Using such a model, the prediction for a tetragonally elongated geometry becomes V_{zz} = −(8/7)e $\langle r^{-3}\rangle_{3d}$. A tetragonally compressed Ni(II) complex is predicted by the same procedure to have V_{zz} = +(4/7)e $\langle r^{-3}\rangle_{3d}$. The net result for a tetrahedral system with an axial compression is a stronger Mössbauer signal at high millimeters per second, while the converse results for a tetrahedral system with an axial elongation.

For the approximately tetrahedral Ni(II) site in *Pf* Rd, we observed an asymmetry in the spectral envelope (a greater dip in transmission at lower mm/s; Figure 3). In contrast, for **3** there is also an asymmetric envelope, but this time with a greater dip in transmission at high millimeters per second. These results indicate an elongated tetrahedral distortion in Ni(II) Rd and an axial compression in **3**. Such findings are consistent with the results from optical MCD spectroscopy,[55] Raman,[56] and the crystal structures.[57] The structural predictions are less clear for the Ni(III) sample, where we saw a loss in the asymmetry of the Mössbauer transmission. This argues for a more spherically symmetric EFG, perhaps due to a combination of geometrical effects and a different electronic configuration.[51] A high-resolution crystal structure could test this hypothesis.

Overall, we find that despite the limited resolution for ^{61}Ni, quadrupole effects can produce a useful broadening and asymmetry of the overall spectral envelope. The asymmetry can in turn be used to determine the sign of V_{zz} for axial systems and thus make predictions about the type of asymmetry at the Ni site.

SUMMARY

Overall, we have demonstrated that ^{61}Ni SR-MS can be an effective tool in studying the magnetic properties and local geometries of ^{61}Ni sites in solid-state materials, coordination complexes, and in Ni metalloproteins. For such dilute samples, the small spot size and low divergence of a synchrotron source are an important factor. One can use cylindrical samples that are several centimeters long and yet only one millimeter in diameter, allowing for modest volumes of precious enzymes. Such a sample configuration is not possible with radioactive sources because of the large source size and divergence. As is usual with synchrotron-based experiments, there is still room for significant improvement in this technique, through brighter sources as well as faster and more efficient detectors. For energy domain experiments, ^{61}Ni SR-MS should thus be a strong competitor to the conventional approach with radioactive sources. At synchrotron sources around the world, both energy- and time-domain nuclear techniques promise exciting opportunities for learning more about Ni chemistry through the special properties of ^{61}Ni.

ASSOCIATED CONTENT

Supporting Information

The Supporting Information is available free of charge on the ACS Publications website at DOI: 10.1021/acs.inorgchem.5b03004.

Nuclear energy levels and lifetimes for ^{61}Ni and typical radioactive sources. Energy levels for pure Zeeman and quadrupole splittings and intermediate case. Predicted spectra for pure Zeeman splittings as a function of magnetic field. Predicted spectra for pure quadrupole splittings. PXRD spectrum for $NiCr_2O_4$. Fit parameters for (**1**) and (**2**). Fit parameters for (**3**) and the rubredoxins. Fit parameters for (**2**) using an unshared V_{zz} value. Fit non-negligible magnetic field fit parameters for (**2**). Non-negligible magnetic field fit parameters for the rubredoxins and (**3**). (PDF)

AUTHOR INFORMATION

Corresponding Author

*E-mail: spjcramer@ucdavis.edu.

Notes

The authors declare no competing financial interest.

ACKNOWLEDGMENTS

This work was supported by the National Institutes of Health (Grant No. GM-65440 to S.P.C), the National Science Foundation (Grant No. CHE-1112035 to C.G.R. and Grant No. CHE-1263760 to P.P.P), and the Deutsche Forschungsgemeinschaft (DFG, Cluster of Excellence UniCat to L.L). Preparation of Ni-rubredoxin samples was supported by the

DOI: 10.1021/acs.inorgchem.5b03004
Inorg. Chem. 2016, 55, 6866−6872

U.S. Department of Energy, Division of Chemical Sciences, Geosciences, and Biosciences, Office of Basic Energy Sciences (DE-FG05-95ER20175 to M.W.W.A). Additional support came from PCOM (to F.E.J), and JSPS KAKENHI (Grant No. 24221005 to M.S). The ^{61}Ni Mössbauer experiments were performed at BL09XU and BL19LXU of SPring-8 with the approval JASRI and RIKEN (Proposal Nos. 2014A1384, 2014B1047, 2015B1175, and 2015B0103). We thank E. Wille and S. Kauzlarich for assistance in the preparation of $^{61}NiCr_2O_4$. We thank Z. Klencsár for assistance with MossWinn.

REFERENCES

(1) *Nickel Alloys;* Heubner, U., Ed.; CRC Press: New York, 2000.
(2) Ralph, J. B. In *Batteries for Sustainability;* Ralph, J. B., Ed.; Springer: New York, 2013; pp 423−443.
(3) Tasker, S. Z.; Standley, E. A.; Jamison, T. F. *Nature* **2014**, *509*, 299−309.
(4) Collinson, S. R.; Schröder, M. In *Encyclopedia of Inorganic and Bioinorganic Chemistry;* John Wiley & Sons, Ltd: New Jersey, 2011.
(5) Ragsdale, S. W. *J. Biol. Chem.* **2009**, *284*, 18571−18575.
(6) Can, M.; Armstrong, F. A.; Ragsdale, S. W. *Chem. Rev.* **2014**, *114*, 4149−4174.
(7) Boer, J. L.; Mulrooney, S. B.; Hausinger, R. P. *Arch. Biochem. Biophys.* **2014**, *544*, 142−152.
(8) Obenshain, F. E.; Wegener, H. H. F. *Phys. Rev.* **1961**, *121*, 1344−1349.
(9) Gütlich, P.; Link, R.; Trautwein, A. X. *Mössbauer Spectroscopy and Transition Metal Chemistry;* Springer-Verlag: Berlin, Germany, 1978; Vol. 3.
(10) Audi, G.; Bersillon, O.; Blachot, J.; Wapstra, A. H. *Nucl. Phys. A* **1997**, *624*, 1−124.
(11) Audi, G.; Wapstra, A. H.; Thibault, C. *Nucl. Phys. A* **2003**, *729*, 337−676.
(12) Gerdau, E. *Hyperfine Interact.* **1994**, *90*, 301−312.
(13) Sergueev, I.; Chumakov, A. I.; Beaume-Dang, T. H. D.; Ruffer, R.; Strohm, C.; van Burck, U. *Phys. Rev. Lett.* **2007**, *99*, 1.
(14) Sergueev, I.; Dubrovinsky, L.; Ekholm, M.; Vekilova, O. Y.; Chumakov, A. I.; Zajac, M.; Potapkin, V.; Kantor, I.; Bornemann, S.; Ebert, H.; Simak, S. I.; Abrikosov, I. A.; Ruffer, R. *Phys. Rev. Lett.* **2013**, *111*, 157601.
(15) Sergueev, I.; Leupold, O.; Wille, H.-C.; Roth, T.; Chumakov, A. I.; R, R. *Physical Review B* **2008**, *78*, 1.
(16) Ruby, S. L. *J. Phys. Colloq.* **1974**, *35*, 209−211.
(17) Gerdau, E.; Rüffer, R.; Winkler, H.; Tolksdorf, W.; Klages, C. P.; Hannon, J. P. *Phys. Rev. Lett.* **1985**, *54*, 835.
(18) Chumakov, A. I.; Zelepukhin, M. V.; Smirnov, G. V.; van Bürck, U.; Rüffer, R.; Hollatz, R.; Rüter, H. D.; Gerdau, E. *Phys. Rev. B: Condens. Matter Mater. Phys.* **1990**, *41*, 9545−9547.
(19) Smirnov, G. V.; van Bürck, U.; Chumakov, A. I.; Baron, A. Q. R.; Rüffer, R. *Phys. Rev. B: Condens. Matter Mater. Phys.* **1997**, *55*, 5811−5815.
(20) Smirnov, G. V.; Zelepukhin, M. V.; Vanburk, W. *JETP Lett.* **1986**, *43*, 352−355.
(21) Mitsui, T.; Seto, M.; Masuda, R.; Kiriyama, K.; Kobayashi, Y. *Jpn. J. Appl. Phys. Lett.* **2007**, *46*, L703−L705.
(22) Mitsui, T.; Seto, M.; Masuda, R. *Jpn. J. Appl. Phys. Lett.* **2007**, *46*, L930−L932.
(23) Seto, M.; Masuda, R.; Higashitaniguchi, S.; Kitao, S.; Kobayashi, Y.; Inaba, C.; Mitsui, T.; Yoda, Y. *Phys. Rev. Lett.* **2009**, *102*, 217602.
(24) Matsuoka, T.; Fujihisa, H.; Hirao, N.; Ohishi, Y.; Mitsui, T.; Masuda, R.; Seto, M.; Yoda, Y.; Shimizu, K.; Machida, A.; Aoki, K. *Phys. Rev. Lett.* **2011**, *107*, 1.
(25) Masuda, R.; Kobayashi, Y.; Kitao, S.; Kurokuzu, M.; Saito, M.; Yoda, Y.; Mitsui, T.; Iga, F.; Seto, M. *Appl. Phys. Lett.* **2014**, *104*, 1.
(26) Nakano, T.; Fukuda, N.; Seto, M.; Kobayashi, Y.; Masuda, R.; Yoda, Y.; Mihara, M.; Nozue, Y. *Physical Review B* **2015**, *91*, 1.
(27) Segi, T.; Masuda, R.; Kobayashi, Y.; Tsubota, T.; Yoda, Y.; Seto, M. *Hyperfine Interact.* **2016**, *237*, 1−5.
(28) Masuda, R.; Kobayashi, Y.; Kitao, S.; Kurokuzu, M.; Saito, M.; Yoda, Y.; Mitsui, T.; Hosoi, K.; Kobayashi, H.; Kitagawa, H.; Seto, M. *Sci. Rep.* **2016**, *6*, 20861.
(29) Gütlich, P.; Bill, E.; Trautwein, A. X. In *Mossbauer Spectroscopy and Transition Metal Chemistry: Fundamentals and Applications;* Springer-Verlag: Berlin, Germany, 2011; pp 235−390.
(30) Okada, T.; Noro, Y.; Kobayashi, Y.; Kitazawa, H.; Ambe, F. *Phys. Lett. A* **1995**, *209*, 241−245.
(31) Klemme, S.; van Miltenburg, J. C. *Phys. Chem. Miner.* **2002**, *29*, 663−667.
(32) Ducelliez, F.; Raynaud, A. *Compt. Rend. Chim.* **1914**, *158*, 2002−2003.
(33) Lin, C. Y.; Guo, J. D.; Fettinger, J. C.; Nagase, S.; Grandjean, F.; Long, G. J.; Chilton, N. F.; Power, P. P. *Inorg. Chem.* **2013**, *52*, 13584−13593.
(34) Rosenfield, S. G.; Armstrong, W. H.; Mascharak, P. K. *Inorg. Chem.* **1986**, *25*, 3014−3018.
(35) Jenney, F. E., Jr.; Adams, M. W. W. *Methods Enzymol.* **2001**, *334*, 45−55.
(36) Moura, I.; Teixeira, M.; Moura, J. J. G.; LeGall, J. *J. Inorg. Biochem.* **1991**, *44*, 127−139.
(37) Yabashi, M.; Mochizuki, T.; Yamazaki, H.; Goto, S.; Ohashi, H.; Takeshita, K.; Ohata, T.; Matsushita, T.; Tamasaku, K.; Tanaka, Y.; Ishikawa, T. *Nucl. Instrum. Methods Phys. Res., Sect. A* **2001**, *467*, 678−681.
(38) Hara, T.; Yabashi, M.; Tanaka, T.; Bizen, T.; Goto, S.; Marechal, X. M.; Seike, T.; Tamasaku, K.; Ishikawa, T.; Kitamura, H. *Rev. Sci. Instrum.* **2002**, *73*, 1125−1128.
(39) Hara, T.; Tanaka, T.; Tanabe, T.; Marechal, X.-M.; Okada, S.; Kitamura, H. *J. Synchrotron Radiat.* **1998**, *5*, 403−405.
(40) Yoda, Y.; Yabashi, M.; Izumi, K.; Zhang, X. W.; Kishimoto, S.; Kitao, S.; Seto, M.; Mitsui, T.; Harami, T.; Imai, Y.; Kikuta, S. *Nucl. Instrum. Methods Phys. Res., Sect. A* **2001**, *467*, 715−718.
(41) Matthias, E.; Schneider, W.; Steffen, R. M. *Phys. Rev.* **1962**, *125*, 261−268.
(42) Kündig, W. *Nucl. Instrum. Methods* **1967**, *48*, 219−228.
(43) Klencsár, Z. *Hyperfine Interact.* **2013**, *217*, 117−126.
(44) Göring, J. *Zeit. Nat. A* **1971**, *26*, 1931.
(45) Göring, J.; Wurtinger, W.; Link, R. *J. Appl. Phys.* **1978**, *49*, 269−272.
(46) Gütlich, P.; Hasselbach, K. M.; Rummel, H.; Spiering, H. *J. Chem. Phys.* **1984**, *81*, 1396−1405.
(47) Bryan, A. M.; Merrill, W. A.; Reiff, W. M.; Fettinger, J. C.; Power, P. P. *Inorg. Chem.* **2012**, *51*, 3366−3373.
(48) Kobayashi, T.; Shimizu, S. *Phys. Lett. A* **1975**, *54*, 311−312.
(49) Seto, M.; Masuda, R.; Higashitaniguchi, S.; Kitao, S.; Kobayashi, Y.; Inaba, C.; Mitsui, T.; Yoda, Y. *J. Phys. Conf. Ser.* **2010**, *217*, 012002.
(50) (a) Lipschutz, M. I.; Tilley, T. D. *Chem. Commun.* **2012**, *48*, 7146−7148. (b) Power, P. P. *Chem. Rev.* **2012**, *112*, 3482−3507. (c) Lipschutz, M. I.; Yang, X.; Chatterjee, R.; Tilley, T. D. *J. Am. Chem. Soc.* **2013**, *135*, 15298−15301. (d) Lin, C. Y.; Fettinger, J. C.; Grandjean, F.; Long, G. J.; Power, P. P. *Inorg. Chem.* **2014**, *53*, 9400−9406.
(51) Huang, Y. H.; Park, J. B.; Adams, M. W. W.; Johnson, M. K. *Inorg. Chem.* **1993**, *32*, 375−376.
(52) Lubitz, W.; Ogata, H.; Rudiger, O.; Reijerse, E. *Chem. Rev.* **2014**, *114*, 4081−4148.
(53) Saint-Martin, P.; Lespinat, P. A.; Fauque, G.; Berlier, Y.; LeGall, J.; Moura, I.; Teixeira, M.; Xavier, A. V.; Moura, J. J. G. *Proc. Natl. Acad. Sci. U. S. A.* **1988**, *85*, 9378−9380.
(54) Slater, J. W.; Shafaat, H. S. *J. Phys. Chem. Lett.* **2015**, *6*, 3731−3736.
(55) Kowal, A. T.; Zambrano, I. C.; Moura, I.; Moura, J. J. G.; LeGall, J.; Johnson, M. K. *Inorg. Chem.* **1988**, *27*, 1162−1166.
(56) Huang, Y. H.; Moura, I.; Moura, J. J. G.; LeGall, J.; Park, J. B.; Adams, M. W. W.; Johnson, M. K. *Inorg. Chem.* **1993**, *32*, 406−412.

DOI: 10.1021/acs.inorgchem.5b03004
Inorg. Chem. 2016, 55, 6866−6872

(57) Maher, M.; Cross, M.; Wilce, M. C.; Guss, J. M.; Wedd, A. G. *Acta Crystallogr., Sect. D: Biol. Crystallogr.* **2004**, *60*, 298−303.

DOI: 10.1021/acs.inorgchem.5b03004
Inorg. Chem. 2016, 55, 6866−6872